The Journal of Antibiotics (2024) 77:278–287
https://doi.org/10.1038/s41429-024-00708-4

Japan Antibiotics Research Association
The Society for Actinomycetes Japan

ARTICLE

Proansamycin B derivatives from the post-PKS modification gene deletion mutant of *Amycolatopsis mediterranei* S699

Xinyu Ma[1] · Feng Ye[1] · Xiaochun Zhang[1] · Zhan Li[1] · Yanjiao Ding[2] · Chunhua Lu[1] · Yuemao Shen[1,3,4]

Received: 7 November 2023 / Revised: 19 January 2024 / Accepted: 23 January 2024 / Published online: 26 February 2024

Abstract

Ten new proansamycin B congeners (**1**–**10**) together with one known (**11**) were isolated and characterized on the basis of 1D and 2D NMR spectroscopic and HRESIMS data from the *Amycolatopsis mediterranei* S699 Δ*PM*::*rifR*+*rif-orf19* mutant. Compounds **8** and **9** featured with six-membered ring and five-membered ring hemiketal, respectively. Compounds **1**, **2**, and **9** displayed antibacterial activity against MRSA (methicillin-resistant *Staphylococcus aureus*), with the MIC (minimal inhibitory concentration) values of 64, 8, and 128 μg/mL, respectively. Compound **1** showed significant cytotoxicity against MDA-MB-231, HepG2 and Panc-1 cell lines with IC_{50} (half maximal inhibitory concentration) values of 2.3 ± 0.2, 2.5 ± 0.3 and 3.8 ± 0.5 μM, respectively.

Introduction

Ansamycins are a class of macrolactams with significant bioactivities, including anti-tuberculosis rifamycins [1], antitumor maytansinoids [2] and geldanamycins [3]. Ansamycins are synthesized by type I polyketide synthase (PKS) that used 3-amino-5-hydroxybenzoic acid (AHBA) as the initial unit for modular loading and embellished through assorted complex post-PKS modifications [4]. Rifamycins were first discovered in 1957, which exhibited bactericidal activities by inhibiting DNA transcription [5]. However, resistance was common in the process of drug overuse and mainly because of target modification and antibiotic inactivation by pathogens [6–8]. Therefore, discovery of new anti-tuberculosis rifamycin derivatives is of particular importance. Five type I polyketide synthases (PKSs: RifA–E) charged for the assemble of undecaketide carbon skeleton, which was then cyclized by the amide synthase RifF to release the first presumable macrocyclic precursor (prorifamycins) [9]. The subsequent post-PKS modifications, which included the dehydrogenation of C-8 hydroxy group and the hydroxylation of C-34 methyl group, resulted in the production of rifamycin W [10, 11]. Then Rif-Orf5 dedicates the transformation from the $\Delta^{12,29}$ olefinic bond of rifamycin W into the ketal. Next, the acetylation of the hydroxy group at C-25 regulated by Rif-Orf20 and the *O*-methylation at C-27 regulated by Rif-Orf14 produced rifamycin SV (R-SV) [12, 13]. The biosynthesis process from R-SV to rifamycin B (R-B) had been thoroughly studied [14]. In this study, *Amycolatopsis mediterranei* S699 Δ*PM*::*rifR*+*rif-orf19* mutant was constructed by deleting post-PKS modification genes to afford ten new congeners of proansamycin B [15] (Fig. 1). These metabolites showed antibacterial and cytotoxic properties. These findings provide direction for the future development of potential anti-MRSA and antitumor drugs by structure modifications of rifamycins based on biosynthesis.

These authors contributed equally: Xinyu Ma, Feng Ye

Supplementary information The online version contains supplementary material available at https://doi.org/10.1038/s41429-024-00708-4.

✉ Yuemao Shen
yshen@sdu.edu.cn

[1] Key Laboratory of Chemical Biology (Ministry of Education), School of Pharmaceutical Sciences, Shandong University, Jinan, Shandong 250012, China

[2] Department of Pharmacy, Shandong Second Provincial General Hospital, Jinan, Shandong 250022, China

[3] State Key Laboratory of Microbial Technology, Shandong University, Qingdao, Shandong 266237, China

[4] NMPA Key Laboratory for Technology Research and Evaluation of Drug Products, Shandong University, Jinan, Shandong 250012, China

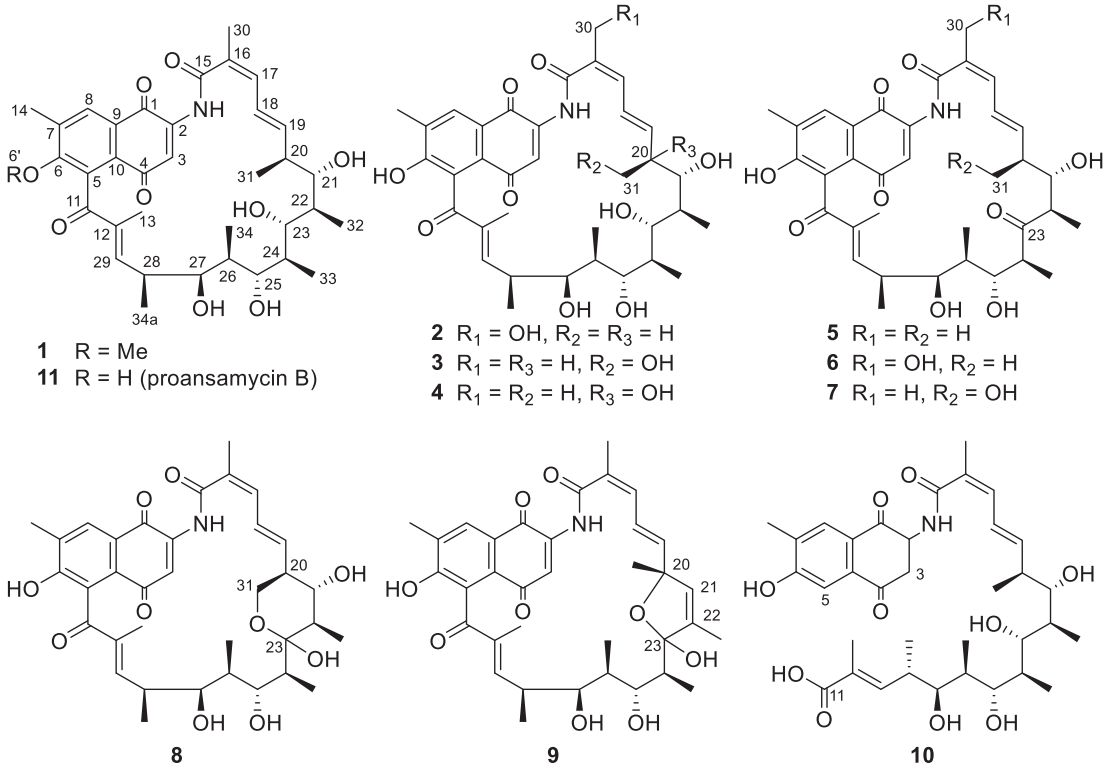

Fig. 1 Structures of proansamycin B and congeners **1–11**

Results and discussion

To explore the modification of rifamycin structure by extra-cluster genes, two post-PKS modification gene fragments within the *rif* gene cluster, namely *rif-orf3* to *rif-orf16* and *rif-orf33*/*rifT*/*rif-orf0*, were deleted to generate the Δ*PM* mutant. The production of rifamycins was totally abolished in the Δ*PM* mutant. Considering the *rif-orf19* gene was involved in the naphthalenic ring formation during rifamycin polyketide assembly, *rif-orf19* was reintroduced together with *rifR* (type II thioesterase gene, deletion reduces metabolite production) into the Δ*PM* mutant to afford the Δ*PM*::*rif-orf19*+*rifR* strain [9]. After culturing on ISP2 agar media for 7 days at 28 °C, the fermentation products of Δ*PM*::*rif-orf19*+*rifR* displayed dissimilar metabolic characteristics from that of the wild-type strain through HPLC and LC-ESI-HRMS analysis. Large scale fermentation (20 L) was conducted, the fermented agar cakes were sliced and extracted. Systematic separation of the extract resulted in the identification of compounds **1**–**11**.

The molecular formula of **1** was confirmed to be $C_{36}H_{47}NO_9$ on the basis of the HRESIMS data at *m/z* 638.3328 $[M+H]^+$ ion (calcd for $C_{36}H_{48}NO_9^+$, 638.3329) (Fig. S7). Comparison of the NMR data of **1** with that of proansamycin B (**11**) (Tables 1, 3, S1 and S11) indicated that **1** was 6-*O*-methyl proansamycin B, which was confirmed by the HMBC correlations from H-6' (δ_H 3.70) to C-6 (δ_C 160.7).

Analysis of the HRESIMS data of compounds **2**, **3** and **4** revealed that they had the same molecular formula of $C_{35}H_{45}NO_{10}$ (Figs. S14, S20 and S27), and one more oxygen atom than that of proansamycin B. Interpretation of the NMR data determined **2**, **3** and **4** to be 30-hydroxy, 31-hydroxy and 20-hydroxyproansamycin B, respectively, which was supported by the presence of C-30 as a hydroxymethyl group (δ_H 4.23, 4.36, δ_C 63.4) (Tables 1, 3 and S2), C-31 as a hydroxymethine (δ_H 3.43, δ_C 62.3) (Tables 1, 3 and S3) and C-20 as a hydroxy-substitued quaternary carbon (δ_C 76.4) (Tables 3 and S4).

The molecular formula of **5** was designated to be $C_{35}H_{43}NO_9$ on the basis of the HRESIMS data at *m/z* 622.3007 $[M+H]^+$ ion (calcd for $C_{35}H_{44}NO_9^+$, 622.3016) (Fig. S34). The NMR comparison with that of proansamycin B (**11**) (Tables 1, 3, S5 and S11) confirmed that **5** was 23-ketoproansamycin B, which was supported by the presence of C-22 (δ_C 48.1), C-23 (δ_C 219.1) and C-24 (δ_C 48.5) (Table 3).

Compounds **6** and **7** had the identical molecular formula of $C_{35}H_{43}NO_{10}$ based on their HRESIMS data (Figs. S41 and S48). The NMR data revealed that both had one more oxygen atom than that of **5**. The NMR comparison determined **6** to be 30-hydroxy-23-ketoproansamycin B on the basis of the presence of C-30 (δ_H 4.23, 4.39, δ_C 63.1) and C-23 (δ_C 219.1) (Tables 2, 3 and S6), and **7** to be 31-hydroxy-23-ketoproansamycin B on the basis of C-31 (δ_H 3.59, δ_C 64.8) and C-23 (δ_C 220.4) (Tables 2, 3 and S7).

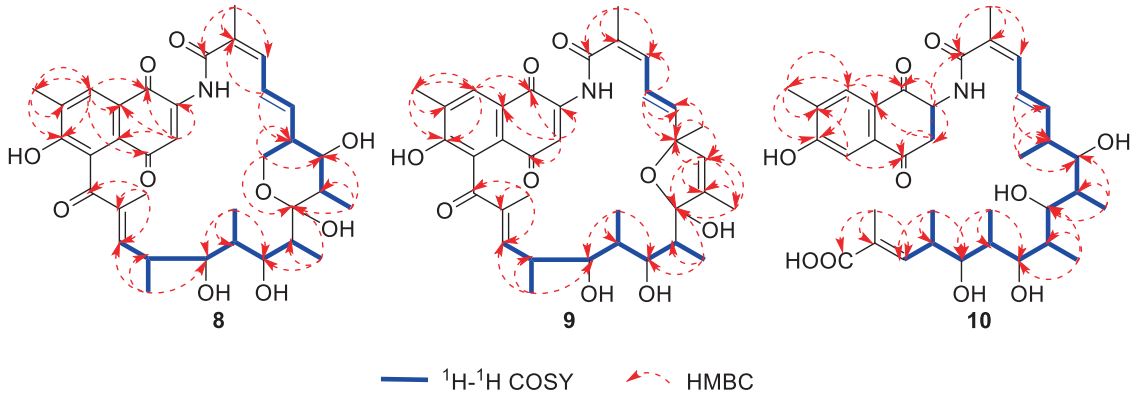

Fig. 2 Selected HMBC (⇢) and ^{1}H-^{1}H COSY (▬) correlations of **8, 9** and **10**

The HRESIMS data at *m/z* 620.2867 $[M + H - H_2O]^+$ ion suggested the molecular formula of **8** to be $C_{35}H_{43}NO_{10}$ (calcd for $C_{35}H_{42}NO_9^+$, 620.2965) (Fig. S55). The existence of a naphthaquinone chromophore was indicated by the HMBC correlations from H-3 (δ_H 7.41) to C-1 (δ_C 179.2), C-2 (δ_C 141.8), C-9 (δ_C 131.1) and C-10 (δ_C 126.0), from H-8 (δ_H 7.86) to C-1, C-4 (δ_C 185.4), C-6 (δ_C 158.7), C-9 and C-14 (δ_C 15.6), and from H-14 (δ_H 2.22) to C-6, C-7 (δ_C 131.4) and C-8 (δ_C 130.2) (Fig. 2 and Tables 2, 3 and S8). The existence of a twenty four-carbon fragment was determined on the basis of the ^{1}H-^{1}H COSY correlations and the HMBC correlations from the H-13 (δ_H 1.85), H-30 (δ_H 1.91), H-31 (δ_H 2.78, 3.13), H-32 (δ_H 0.97), H-33 (δ_H 0.89), H-34 (δ_H 0.41) and H-34a (δ_H 0.95) to the corresponding carbons. The hydroxylation of C-31 and oxidation of C-23 to a carbonyl group followed by the hemiketalization with the C-31 hydroxy group was confirmed on the basis of the HMBC correlations from H-31 to C-23 (δ_C 102.9) (Table 3, Fig. 2). The connectivity between C-5 and C-11 and the amide bond linkage between C-2 and C-15 was deduced on the basis of biosynthetic logic together with the HRESIMS data. Therefore, with the aid of biosynthetic logic and optical rotation comparisons, the structure of **8** was identified [16, 17].

Compound **9** had the molecular formula $C_{35}H_{41}NO_9$ on the basis of the HRESIMS data *m/z* 602.2748 $[M + H - H_2O]^+$ ion (calad for $C_{35}H_{40}NO_8^+$, 602.2860) and 642.2674 $[M + Na]^+$ (calcd for $C_{35}H_{41}NO_9Na^+$, 642.2679) (Fig. S62). A naphthaquinone chromophore was established by the HMBC correlations from H-3 (δ_H 6.06) to C-1 (δ_C 179.1), C-2 (δ_C 140.7), C-4 (δ_C 184.5) and C-9 (δ_C 132.7), from H-8 (δ_H 7.95) to C-1, C-6 (δ_C 158.6), C-9 and C-14 (δ_C 15.4), and from H-14 (δ_H 2.33) to C-6, C-7 (δ_C 131.5) and C-8 (δ_C 130.3) (Tables 2, 3 and S9, Fig. 2). The HMBC correlations from the H-13 (δ_H 1.89), H-30 (δ_H 2.06), H-31 (δ_H 1.21), H-32 (δ_H 1.19), H-33 (δ_H 0.73), H-34 (0.52), H-34a (δ_H 0.79) to the corresponding carbons and ^{1}H-^{1}H COSY correlations (Fig. 2 and Table S9) indicated the presence of a twenty four-carbon fragment. The connectivity between C-5 (δ_C 121.9) and C-11 and the amide bond linkage between C-2 and C-15 was deduced on the basis of biosynthetic logic together with the HRESIMS data. The C-23 hydroxymethine was oxidized to carbonyl that formed a hemiketal with the C-20 hydroxy group was revealed on the basis of the ^{13}C NMR of C-23 (δ_C 112.2) (Table 3, Fig. 2). Therefore, the structure of **9** was determined.

The molecular formula of **10** was elucidated to be $C_{35}H_{49}NO_{10}$ on the basis of the HRESIMS data *m/z* 644.3430 $[M + H]^+$ ion (calcd for $C_{35}H_{50}NO_{10}^+$, 644.3435) (Fig. S69). Interpretation the NMR data of **10** exhibited the presence of a dihydronaphthoquinone chromophore in consideration of the presence of the extra protons H-2 (δ_H 5.20) and H-3 (δ_H 3.25) (Table 2). That the *ansa* chain occurred a retro-Claisen cleavage between C-5 and C-11 was revealed on the basis of the ^{13}C NMR of C-11 (δ_C 170.6) and the extra aromatic proton H-5 (δ_H 7.34) compared to that of normal rifamycins, which was confirmed by the HMBC correlations from H-5 to C-4 (δ_C 194.2) and C-7 (δ_C 132.9) (Tables 3 and S10). A twenty four-carbon fragment was established on the basis of the ^{1}H-^{1}H COSY, and HMBC correlations from the H-13 (δ_H 1.85), H-30 (δ_H 2.00), H-31 (δ_H 1.02), H-32 (δ_H 0.94), H-33 (δ_H 0.96), H-34 (δ_H 0.80), H-34a (δ_H 0.95) to the corresponding carbons (Fig. 2). The amide bond linkage between C-2 (δ_C 53.8) and C-15 was deduced according to the intense correlations of HMBC from the H-2 to C-15. Based on the biosynthetic logic, the NOESY correlations (Fig. S68) and the optical rotation comparison with that of proansamycin B-M1 [17], the stereochemistry of aliphatic carbons of **10** was considered to be the same as that of proansamycin B (**11**).

The antimicrobial activity of compounds **1–11** was assayed against *Pseudomonas aeruginosa* PA01, methicillin-resistant *Staphylococcus aureus* (MRSA), *Proteusbacillus vulgaris* CPCC 160013 and *Mycobacterium smegmatis* mc^2 155, respectively. The results indicated that only **1, 2** and **9** exhibited inhibitory activity against MRSA. These compounds were further measured

Table 1 ^{1}H NMR Spectroscopic Data (400 MHz, CD_3OD) of compounds **1**–**5** (δ_H, *J* in Hz)[a]

No.	1	2	3	4	5
3	7.57 (s)	7.60 (s)	7.50 (s)	7.58 (s)	7.58 (s)
8	7.97 (s)	7.94 (s)	7.85(s)	7.96 (s)	7.93 (s)
13	1.94 (s)	2.05 (s)	1.94 (s)	2.04 (s)	2.01 (s)
14	2.36 (s)	2.36 (s)	2.26 (s)	2.37 (s)	2.35 (s)
17	6.14 (d, 9.5)	6.51 (d, 11.0)	6.19 (d, 10.9)	6.26 (d, 10.8)	6.22 (d, 10. 4)
18	6.40 (dd, 11.0, 15.9)	6.91 (dd, 11.0, 16.2)	6.43 (dd, 11.0, 15.8)	6.49 (dd, 10.9, 15.9)	6.07 (dd, 10.8, 15.1)
19	5.98 (dd, 6.7, 15.9)	6.37 (dd, 7.0, 16.0)	5.91 (dd, 7.1, 15.8)	5.96 (d, 16.0)	5.83 (dd, 9.5, 15.1)
20	2.26 (m)	2.40 (m)	2.36 (m)		1.85 (m)
21	3.93 (d)	4.04 (m)	4.15 (m)	3.95 (s)	3.58 (d, 9.3)
22	1.77 (m)	1.90 (m)	1.85 (m)	2.01 (m)	2.87 (m)
23	3.37 (m)	3.49 (m)	3.36 (m)	3.42 (dd, 8.8, 1.7)	
24	1.68 (m)	1.80 (m)	1.66 (m)	1.72 (m)	2.48 (m)
25	3.87 (m)	3.95 (d, 10.0)	3.85 (d, 10.2)	3.91 (d, 10.7)	3.83 (d, 10.3)
26	1.33 (m)	1.43 (m)	1.32 (m)	1.43 (m)	1.34 (m)
27	3.88 (s)	4.01 (s)	3.87 (s)	3.96 (s)	4.00 (s)
28	2.51 (m)	2.65 (m)	2.53 (m)	2.62 (m)	2.56 (m)
29	6.27 (d, 9.3)	6.43 (d, 9.6)	6.31 (d, 9.3)	6.36 (d, 9.2)	6.31 (d, 8.9)
30	1.98 (s)	4.23 (d, 12.1) 4.36 (d, 12.0)	1.98 (s)	2.10 (s)	2.04 (s)
31	0.81 (d, 7.0)	0.95 (d, 7.0)	3.43 (m)	1.22 (s)	1.05 (m)
32	0.95 (d, 5.9)	1.05 (m)	0.97 (d,7.0)	1.15 (d, 6.9)	1.04 (m)
33	0.62 (d, 6.8)	0.74 (d, 6.8)	0.63 (d, 6.8)	0.75 (d, 6.8)	1.11 (d, 7.3)
34	0.25 (d, 7.0)	0.39 (d, 7.0)	0.27 (d, 7.0)	0.40 (d, 6.9)	0.36 (d, 7.1)
34a	0.97 (d, 6.0)	1.07 (m)	0.95 (d, 7.1)	1.04 (d, 7.0)	1.01 (m)
6'	3.70 (s)				

[a]*s* singlet, *d* doublet, *dd* double doublet, *t* triplet, *m* multiplet

by the microbroth dilution method, giving the MIC values of 64, 8 and 128 μg/mL for **1, 2** and **9**, respectively (Table S12).

The cytotoxicity of compounds **1**–**11** was assayed by CCK-8 method (Bimake, USA) while adriamycin was used as the positive control. Only compound **1** exhibited significant inhibitory activity against the proliferation of MDA-MB-231, HepG2 and Panc-1 cells (Table 4). After exposure to **1** (2.5 μM) for 24 h, the percentage of annexin V-positive MDA-MB-231 cells was increased (46.04%). Flow cytometry analysis indicated a dose-dependent manner (Figs. S70 and S71).

The isolation of **1**–**11** from the *A. mediterranei* S699Δ*PM*::*rifR*+*rif-orf19* mutant indicated that Rif-Orf19 was sufficient for the formation of the naphthalenic ring with the aid of non-enzymatic oxidation of hydroquinone and the followed Michael addition (Fig. 3). This result was significant in that our previous inactivation of the *rif-orf19* gene in *A. mediterranei* S699 led to disrupting the production of rifamycins and their anticipated benzenic precursors, which was discrepant to the isolation of benzenic precursors of neoansamycins from the deletion mutant of the *nam7* gene, a homolog of the *rif-orf19* gene [18]. All compounds featured without C-8 hydroxy group substitution, supporting the previous conclusion that proansamycin B was an intermediate of the 8-deoxy variant shunt pathway of rifamycin B biosynthesis. The presence of C-34a methyl group indicated that its hydroxylation was specifically catalyzed by an enzyme encoded by a gene in the *rif* cluster rather than by a house-keeping oxidase (Fig. 3) [19]. Compounds **8** and **9** featured with a six-membered ring and a five-membered ring hemiketal, respectively, showing the involvement of non-enzymatic conversion in derivatizing rifamycins. Compound **10** experienced C-5/C-11 retro-Claisen cleavage during the biosynthesis process as exemplified by that of proansamycin B-M1 [17] and proto-rifamycin I–M1 [20], hygrocins I and J [21], divergolides R and S [22] and microansamycins G–I [23]. Compared with proansamycin B, compounds **2**–**7** illustrated diverse oxygenations at different carbons including C-20, C-23, C-30 and C-31, indicating that the *ansa* chain of rifamycins are easily oxidized at these specific sites (Fig. 3).

Table 2 ^{1}H NMR Spectroscopic Data (400 MHz, CD_3OD) of compounds **6–10** (δ_H, J in Hz)[a]

No.	6	7	8	9	10
2					5.20 (dd, 6.6, 11.8)
3	7. 55 (s)	7. 60 (s)	7.41 (s)	6.06 (s)	3.25 (m)
5					7.34 (s)
8	7.94 (s)	7.94 (s)	7.86 (s)	7.95 (s)	7.85 (s)
13	2.02 (s)	2.01 (s)	1.85 (s)	1.89 (s)	1.85 (s)
14	2.36 (s)	2.37 (s)	2.22 (s)	2.33 (s)	2.31 (s)
17	6.46 (m)	6.26 (d, 11.0)	6.05 (d, 7.2)	6.03 (d, 11.2)	6.25 (d, 11.2)
18	6.39 (m)	6.13 (dd, 11.2, 15.1)	5.88 (dd, 5.6, 15.9)	5.81 (dd, 11.1, 15.4)	6.87 (dd, 11.1, 15.2)
19	6.04 (dd, 8.9, 15.0)	5.82 (dd, 9.9, 15.1)	5.26 (dd, 8.7, 15.7)	5.94 (dd, 8.7, 15.7)	5.90 (dd, 8.0, 15.1)
20	1.98 (m)	1.87 (m)	2.01 (m)		2.48 (m)
21	3.74 (m)	3.81 (d, 10.6)	3.25 (m)	5.73 (d, 1.7)	3.81(d, 9.0)
22	2.95 (m)	2.94 (m)	1.61 (m)		1.96 (m)
23					3.62 (d, 5.9)
24	2.69 (m)	2.47 (m)	1.47 (m)	1.59 (m)	1.85 (m)
25	3.80 (d, 11.0)	3.85 (d, 10.7)	3.65 (dd, 4.5, 12.0)	3.56 (dd, 4.9, 11.1)	4.05 (d, 9.9)
26	1.36 (m)	1.34 (m)	1.66 (m)	1.74 (m)	1.80 (m)
27	4.01 (m)	4.00 (s)	3.83 (s)	3.70 (m)	3.85 (d, 8.5)
28	2.59 (m)	2.57 (m)	2.55 (m)	2.55 (m)	2.75 (m)
29	6.33 (m)	6.32 (d, 8.7)	6.47 (d, 8.6)	6.53 (d, 8.6)	6.82 (d, 9.8)
30	4.23 (m), 4.39 (m)	2.05 (s)	1.91 (s)	2.06 (s)	2.00 (s)
31	1.08 (d, 6.8)	3.59 (m)	3.13 (t, 11.5) 2.78 (dd, 5.30, 11.0)	1.21 (s)	1.02 (d, 6.8)
32	1.04 (d, 7.1)	1.07 (d, 6.8)	0.97 (d, 4.9)	1.19 (s)	0.94 (d, 7.0)
33	1.13 (d, 7.3)	1.12 (d, 7.4)	0.89 (d, 7.1)	0.73 (d, 6.7)	0.96 (d, 5.5)
34	0.42 (d, 7.0)	0.37 (d, 7.0)	0.41 (d, 7.0)	0.52 (d, 7.0)	0.80 (d, 7.0)
34a	1.02 (d, 7.7)	1.04 (d, 7.1)	0.95 (d, 5.2)	0.79 (d, 7.1)	0.95 (d, 5.2)

[a]*s* singlet, *d* doublet, *dd* double doublet, *t* triplet, *m* multiplet

Conclusion

In the present study, the fermentation products of the mutant strain Δ*PM*::*rifR*+*rif-orf19* were systematically isolated. The main product proansamycin B (**11**) and its ten new derivatives were obtained. Some of them had good antibacterial activity and cytotoxicity. The complex post-PKS modifications of rifamycins play a key role in enriching structural diversity and enhancing bioactivity [24]. In addition to the reported enzyme-mediated modifications, there are also a large number of non-specific modifications that are masked by the rifamycin B synthesis pathway, endowing rifamycins further structure diversity and biological activity.

Experimental section

Strains and plasmids

The strain used in the work was *Amycolatopsis mediterranei* S699, which was firstly separated in 1957 at St. Raphael, France, as a gift from Heinz G. Floss laboratory at University of Washington, Seattle. Firstly, the gene fragment of *rif-orf3* to *rif-orf16* was disturbed through homologous recombination and insertion into the shuttle plasmid pOJ260 of the *E. coli-Micromonospora* (Fig. S74) and the mutant of Δ*orf3-orf16* was selected by apramycin resistance. Secondly, the fragment of *rif-orf33-rifT-rif-orf0* was removed on the basis of Δ*orf3-orf16* mutant according to the above method to obtain Δ*PM* mutant. To avoid the influence of polarity effects, the promotor *rifKp* was replenishmented to the gene deleted region during the construction of Δ*PM* mutant (Fig. S72). We verified Δ*PM* mutant using polymerase chain reaction (PCR) method (Fig. S75) along with a pair of primers on the genome and plasmid (Table S13). Finally, *rifR* and *rif-orf19* genes were transformed into Δ*PM* mutant with electroporation technology to build a novel strain of *A. mediterranei* S699 Δ*PM*::*rifR*+*rif-orf19*. These strains need to grow on YMG (yeast extract 4 g, malt extract 10 g, glucose 4 g, 20 g agar, double distilled H_2O 1000 mL, pH 7.2) agar media and be inverted in an incubator at 28 °C for product productions.

Table 3 ^{13}C NMR Spectroscopic Data (100 MHz, CD_3OD) of compounds **1**–**10** (δ_C)[a]

No.	1	2	3	4	5	6	7	8	9	10
1	179.3s	179.2s	179.0s	180.6s	179.0s	179.2s	180.5s	179.2s	179.1s	192.5s
2	140.6s	140.6s	140.5s	142.0s	140.5s	140.4s	142.0s	141.8s	140.7s	53.8d
3	117.4d	116.7d	117.1d	118.6d	117.5d	117.5d	119.2d	114.4d	116.6d	43.4t
4	185.2s	186.0s	185.9s	187.4s	185.9s	186.0s	187.4s	185.4s	184.5s	194.2s
5	126.6s	127.5s	122.7s	124.0s	122.5s	122.4s	124.1s	121.9s	121.9s	110.1d
6	160.7s	158.7s	158.3s	160.1s	158.6s	158.5s	159.9s	158.7s	158.6s	161.6s
7	129.7s	131.5s	131.1s	133.1s	130.9s	130.8s	133.3s	131.4s	131.5s	132.9s
8	130.8d	130.2d	130.3d	131.8d	130.2d	130.1d	131.7d	130.2d	130.3d	129.7d
9	138.4s	135.2s	130.2s	132.1s	131.7s	131.7s	132.4s	131.1s	132.7s	135.6s
10	134.3s	133.1s	131.5s	128.6s	126.5s	126.6s	128.1s	126.0s	126.0s	130.1s
11	198.1s	199.5s	199.4s	200.8s	199.0s	199.0s	200.6s	198.2s	198.4s	170.6s
12	136.5s	136.8s	136.8s	138.6s	137.7s	137.7s	139.3s	135.2s	135.8s	127.1s
13	10.3q	10.3q	10.5q	12.0q	10.6q	10.5q	12.2q	9.2q	9.7q	11.4q
14	15.5q	15.6q	15.7q	17.1q	15.6q	15.6q	17.2q	15.6q	15.4q	15.1q
15	170.9s	169.0s	171.1s	171.5s	171.3s	169.3s	172.9s	171.8s	171.3s	171.1s
16	130.7s	132.4s	127.3s	132.7s	131.6s	134.1s	133.7s	133.4s	130.0s	126.7s
17	133.5d	138.0d	133.4d	135.6d	131.8d	134.9d	132.9d	129.0d	129.6d	132.9d
18	124.7d	125.5d	127.2d	125.6d	125.8d	126.0d	130.1d	127.8d	122.0d	126.8d
19	140.0d	144.4d	136.1d	147.7d	139.1d	142.5d	136.3d	134.0d	144.5d	141.0d
20	37.7d	37.6d	46.3d	76.4s	41.8d	41.0d	52.3d	49.6d	86.7s	40.8d
21	73.3d	74.8d	70.4d	76.1d	76.8d	76.4d	73.7d	73.2d	129.1d	74.4d
22	33.0d	32.9d	33.7d	34.8d	48.1d	47.9d	49.6d	44.2d	137.9s	36.3d
23	77.5d	77.6d	77.7d	80.1d	219.1s	219.1s	220.4s	102.9s	112.2s	77.8d
24	36.5d	36.5d	36.8d	38.2d	48.5d	47.0d	50.5d	41.9d	34.6d	35.1d
25	69.8d	70.0d	70.0d	71.8d	69.7d	70.2d	71.2d	72.8d	72.5d	71.1d
26	42.6d	42.7d	42.4d	43.6d	41.0d	41.0d	42.5d	40.0d	40.5d	38.0d
27	72.6d	72.8d	72.7d	74.4d	72.0d	72.1d	73.4d	78.8d	74.5d	73.8d
28	39.6d	40.0d	39.6d	41.1d	39.1d	39.4d	40.7d	38.0d	36.6d	37.0d
29	146.2d	144.9d	145.2d	146.6d	144.4d	144.6d	146.0d	147.5d	148.1d	146.7d
30	18.8q	63.4d	18.8q	20.3q	18.9q	63.1d	20.4q	19.2q	19.0q	19.3q
31	16.6q	16.3q	62.3t	26.0q	18.6q	18.1q	64.8t	63.2t	24.7q	16.0q
32	13.7q	9.5q	10.9q	13.7q	13.2q	11.6q	15.3q	12.5q	10.2q	9.1q
33	7.5q	7.4q	7.4q	9.2q	6.8q	7.1q	8.2q	11.0q	11.1q	9.2q
34	9.8q	9.7q	9.9q	11.2q	10.0q	9.8q	11.6q	5.1q	4.3q	8.1q
34a	18.1q	17.9q	17.9q	19.1q	18.1q	18.0q	19.5q	17.7q	19.0q	15.6q
6’	61.4q									

[a]*s* quaternary carbon, *d* tertiary carbon, *t* secondary carbon, *q* primary carbon

Escherichia coli DH5α strain was leveraged to conduct plasmid reproduction. *E. coli* cells were growing in Luria-Bertani (LB) medium (tryptone 10 g, yeast extract 5 g, NaCl 10 g, ddH_2O 1000 ml, pH 7.2) and in an incubator at 37 °C. A final concentration of 50 μg/mL antibiotic apramycin was added to the LB medium of all cultivated strains. Mixing of mycelium with 20% glycerol and retained at –80 °C.

Throughout the entire study, the suicide vector pOJ260 (containing *aac (3) IV, oriT, rep^{PUC}, lacZ*) was used to inactivate genes within the framework. The gene expression in the Δ*PM*::*rifR*+*rif-orf19* strain was completed through the integration vector pSET152 (containing *aac (3) IV, oriT (RK2), ori (pUC18), int (φC31), attP (φC31), lacZα*).

DNA manipulation

Compete the gene knock-out plasmid according to the following steps. Firstly, we used the *A. mediterranei* S699 genomic DNA as a template and amplified the upstream and downstream homologous arms (approximately 2 kb) of the

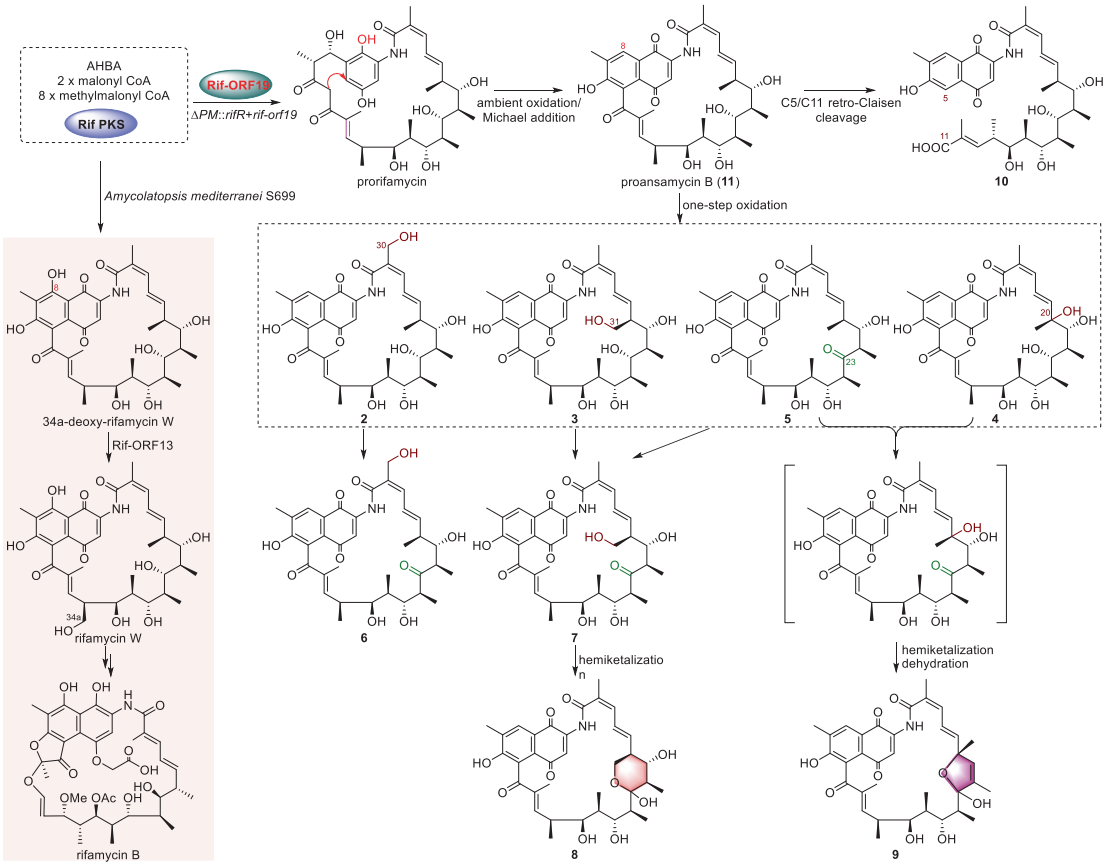

Fig. 3 Proposed biosynthetic pathway of compounds isolated from the *A. mediterranei* S699Δ*PM*::*rifR*+*rif-orf19* mutant

Table 4 Cytotoxicity of Compound **1** and Adriamycin (IC_{50} in μM)[a]

Cell line	**1**	adriamycin
MDA-MB-231	2.3 ± 0.2	1.2 ± 0.5
HepG2	2.5 ± 0.3	1.5 ± 0.5
Panc-1	3.8 ± 0.5	1.5 ± 0.3
L0-2	16.5 ± 0.5	8.5 ± 0.5

[a]Cells were treated for 48 h with compound **1** and adriamycin, respectively. The viability values were determined by CCK8 assays. Results were expressed as means of three independent experiments

target genes through PCR. Inserting the purified PCR fragments into linearized vector pOJ260 through Gibson assembly. Then chemically transformed the assembled product into 100 μL DH5α competent cells and identification of positive clones through resistance screening and DNA sequencing (Fig. S72). We used the same method as Ding et al. to delete Target genes. Plasmid was reproduced in DH5α and converted into *A. mediterranei* S699 competent cells through electroporation technology. Screening the recombinants produced by homologous recombination of knock-out plasmid and *A. mediterranei* S699 genomic DNA, transferring it into apramycin-free YMG agar for several rounds of non-selective growth (Fig. S73). Gene knockout validation was performed using PCR to screen recombinants of apramycin-sensitive from double-crossover recombination (Fig. S74). Please refer to the Supplementary Information for the specific process.

The integrating vector pSET152 was served for gene complementation in the strain of *A. mediterranei* S699 Δ*PM*::*rif-orf19*+*rifR*. The production of pSET152-*rifK*p was achieved by inserting the *rifK* promoter fragment and synthesized after digestion by NdeI and XbaI into the pSET152 vector pretreated by XbaI. Using *A. mediterranei* S699 genomic DNA as a template, both *rif-orf19* and *rifR* genes were amplified by PCR. The PCR fragments of NdeI/EcoRI *rif-orf19* and *rifR* were inserted downstream of the *rifK*p promoter in pSET152, respectively. The identification of positive clones were completed through PCR screening and DNA sequencing. Then, *rifK*p-*rif-orf19* fragment was amplified by PCR using pSET152-*rifK*p-*rif-orf19* as a template and inserted into linearized pSET152-*rifK*p-*rifR* downstream by EcoRI. The final strain of *A. mediterranei* S699 Δ*PM*::*rifR*+*orf19* was obtained by electroporation of the resultant plasmid pSET152-*rifK*p-*rifR*-*rifK*p-*rif-orf19* into *A. mediterranei* S699 Δ*PM* competent cells.

HPLC detection and analysis of the metabolites in mutant strains

The *A. mediterranei* S699 Δ*PM*::*rifR*+*rif-orf19* strain was inoculated on YMG agar petri dishes and grew for 7 days in 28 °C incubator. The diced culture was extracted at room temperature overnight with EtOAc/MeOH (4 : 1, *v*/*v*). A small amount of concentrated crude extract was dissolved in an appropriate volume of methanol and analyzed through HPLC. The HPLC solvents included (A) $ddH_2O + 0.5\%$ formic acid and (B) acetonitrile, UV detection was monitored at 254 nm and the flow rate was 1 mL/min. First 5 min were eluted with 20% A to 35% B gradient, the 5–15 min were eluted with 35% A to 55% B gradient, the 15–19 min were eluted with 55% A to 65% B gradient, the 19–23 min were eluted with 65% A to 100% B gradient, and finally eluted with a 100% B gradient for 4 min (Fig. S76 and S77).

General experimental procedures

NMR spectra were measured using Bruker 400 MHz and/or AVANCE 600 MHz NMR spectrometers. Column chromatography (CC) was performed on reversed-phase (RP) C_{18} silica gel (Merck, Darmstadt, Germany). Semi-preparative HPLC was performed on Agilent 1200 (Agilent Eclipse XDB-C_{18}, 5 μm, 9.4 × 250 mm). Optical rotations were measured with the instrument of Auton Paar MCP200 Automatic Polarimeter. HRESIMS data were obtained with the instrument of LTQ-Orbitrap XL (Thermo Scientific, Waltham, MA, USA).

Fermentation, extraction and isolation of the metabolites in mutants

The *A. mediterranei* S699 Δ*PM*::*rifR*+*rif-orf19* mutant was inoculated onto 20 L YMG agar plates and grew for 7 days in 28 °C incubator. The diced culture of 20 L was extracted at room temperature with EtOAc/MeOH (4 : 1, *v*/*v*) three times overnight. The crude extract was partitioned between EtOAc and H_2O (1 : 1, *v*/*v*) until the EtOAc layer was almost colorless. The organic extract was separated on RP C_{18} silica gel (130 g) by medium-pressure liquid chromatography (MPLC). Gradient elution was performed with 500 mL of 30%, 50%, 70%, and 100% CH_3CN to obtain five fractions (Frs.), A–E. The fractions were further separated by semi-preparative HPLC, the flow rate for HPLC was 4 mL/min and the UV absorption was monitored at 254 nm.

Compound **3** (t_R 15.0 min, 9.5 mg) was obtained by semi-preparative HPLC from Fr. A (0.11 g) under the condition of 28% CH_3CN elution. Fr. B (0.12 g) was purified by semi-preparative HPLC with 40% CH_3CN to give **7** (t_R 8.2 min, 12.0 mg). Fr. C (0.39 g) was separated by semi-preparative HPLC with 42% CH_3CN to afford **2** (t_R 7.2 min, 6.2 mg), **6** (t_R 8.9 min, 9.4 mg), **4** (t_R 11.1 min, 10.5 mg), **8** (t_R 13.8 min, 10.2 mg) and **10** (t_R 18.6 min, 10.3 mg), respectively. Fr. D (0.42 g) was separated by semi-preparative HPLC with 45% CH_3CN to obtain **11** (t_R 7.8 min, 36.7 mg), **5** (t_R 11.4 min, 6.6 mg) and **1** (t_R 12.9 min, 9.8 mg), respectively. Compound **9** (t_R 17.5 min, 16.7 mg) was purified from Fr. E (0.28 g) by semi-preparative HPLC with 52% CH_3CN.

Compound **1**: yellow powder; $[\alpha]^{20}D + 60.1$ (*c* 0.1, MeOH); UV (MeOH) λ_{max} (logε) 229 (3.00), 266 (2.70), 300 (1.54) nm; for ^1H and ^{13}C NMR data, see Tables 1 and 3; HRESIMS: *m/z* 638.3328 $[M + H]^+$ (calcd for $C_{36}H_{48}NO_9^+$, 638.3324).

Compound **2**: tawny powder; $[\alpha]^{20}{}_D = +34.7$ (*c* 0.10, MeOH); UV (MeOH) λ_{max} (logε) 215 (3.04), 215 (2.96), 274 (2.88) nm; for ^1H and ^{13}C NMR data, see Tables 1 and 3; HRESIMS: *m/z* 640.3116 $[M + H]^+$ (calcd for $C_{35}H_{46}NO_{10}^+$, 640.3116).

Compound **3**: dark brown powder; $[\alpha]^{20}{}_D = +135.5$ (*c* 0.10, MeOH); UV (MeOH) λ_{max} (logε) 228 (2.76), 271 (2.13), 309 (1.12)nm; for ^1H and ^{13}C NMR data, see Tables 1 and 3; HRESIMS: *m/z* 640.3125 $[M + H]^+$ (calcd for $C_{35}H_{46}NO_{10}^+$, 640.3116).

Compound **4**: tawny powder; $[\alpha]^{20}{}_D = +98.1$ (*c* 0.10, MeOH); UV (MeOH) λ_{max} (logε) 230 (2.49), 273 (2.13), 309 (1.12) nm; for ^1H and ^{13}C NMR data, see Tables 1 and 3; HRESIMS: *m/z* 662.2938 $[M + Na]^+$ (calcd for $C_{35}H_{45}NO_{10}Na^+$, 662.2936).

Compound **5**: yellow powder; $[\alpha]^{20}{}_D = +175.5$ (*c* 0.10, MeOH); UV (MeOH) λ_{max} (logε) 228 (2.80), 267 (2.07), 309 (1.12) nm; for ^1H and ^{13}C NMR data, see Tables 1 and 3; HRESIMS: *m/z* 622.3007 $[M + H]^+$ (calcd for $C_{35}H_{44}NO_9^+$, 622.3011).

Compound **6**: tawny powder; $[\alpha]^{20}{}_D = +162.2$ (*c* 0.10, MeOH); UV (MeOH) λ_{max} (logε) 215 (3.62), 231 (3.67), 271 (3.32) nm; for ^1H and ^{13}C NMR data, see Table 2 and 3; HRESIMS: *m/z* 638.2970 $[M + H]^+$ (calcd for $C_{35}H_{44}NO_{10}^+$, 638.2960).

Compound **7**: tawny powder; $[\alpha]^{20}{}_D = +94.1$ (*c* 0.10, MeOH); UV (MeOH) λ_{max} (logε) 227 (3.88), 309 (2.15) nm; for ^1H and ^{13}C NMR data, see Tables 2 and 3; HRESIMS: *m/z* 638.2955 $[M + H]^+$ (calcd for $C_{35}H_{44}NO_{10}^+$, 638.2960).

Compound **8**: yellow powder; $[\alpha]^{20}{}_D = -226.9$ (*c* 0.10, MeOH); UV (MeOH) λ_{max} (logε) 223 (3.99), 311 (2.21) nm; for ^1H and ^{13}C NMR data, see Tables 2 and 3; HRESIMS: *m/z* 620.2867 $[M + H - H_2O]$ (calcd for $C_{35}H_{42}NO_9$, 620.2965).

Compound **9**: yellow powder; $[\alpha]^{20}{}_D = -172.9$ (*c* 0.10, MeOH); UV (MeOH) λ_{max} (logε) 219 (2.91), 310 (0.69) nm; for ^1H and ^{13}C NMR data, see Tables 2 and 3;

HRESIMS: *m/z* 602.2748 $[M + H - H_2O]$ (calcd for $C_{35}H_{40}NO_8$, 602.2860), and 642.2674 $[M + Na]^+$ (calcd for $C_{35}H_{41}NO_9Na^+$, 642.2674).

Compound **10**: yellow powder; $[\alpha]^{20}_D = +33.4$ (*c* 0.10, MeOH); UV (MeOH) λ_{max} (logε) 249 (2.61) nm; for ^1H and ^{13}C NMR data, see Tables 2 and 3; HRESIMS: *m/z* 628.3484 $[M + H]^+$ (calcd for $C_{35}H_{50}NO_{10}^+$, 628.3480).

Antimicrobial assay

Compounds **1**–**11** against methicillin-resistant *Staphylococcus aureus* (MRSA) were assayed by paper disc diffusion assay in Shandong Second Provincial General Hospital. The positive control was vancomycin. The tested compounds (40 μg each) wer immersed onto the paper disks (Ø6 mm) that were then placed on the agar plates inoculated with MRSA. The test plates were incubated for 24 h at 37 °C and checked for the formation of bacteriostatic circles. The minimal inhibitory concentration (MIC) values of active compounds on MRSA growth were measured using the microbroth dilution method. Bacteria were grown in the LB media and the optical density measured at 600 nm was approximately 0.2. Equipped with 100 μL flat-bottomed microdilution trays for serial diluted compounds were inoculated into 100 μL bacteria suspensions, ultimately forming 1.0×10^3 colony forming units (CFU)/mL (spectrophotometer at 600 nm) of an inoculum size.

Cytotoxicity assay

The in vitro cytotoxicity was measured on four cell lines: L02, MDA-MB-231, HepG2, and Panc-1, respectively. All cell lines were purchased from Cell Bank of the Institute of Biochemistry and Cell Biology, China Academy of Sciences (Shanghai, China), and cultured under the standard conditions. According to the manufacturer's instructions, cell-grown inhibition was assayed by Cell Counting Kit-8 (CCK-8) (Bimake, USA). Using adriamycin as the positive control, approximately 7×10^3 per well were seeded in 96-well plates and treated with different concentrations of compounds **1**–**11** for 48 h, and 10 μL of CCK-8 was added to each well and incubated for 4 h. The absorbance was measured through Spark 30086376 (TECAN, Austria), and IC_{50} values were calculated using software Prism 7 (GraphPad Software, Inc., San Diego, CA, USA).

Funding This research was supported by the National Key Research and Development Program (2019YFA0905402), the National Natural Science Foundation of China (81673317, 81602979, 81530091), the Program for Changjiang Scholars and Innovative Research Team in University (IRT_17R68).

Compliance with ethical standards

Conflict of interest The authors declare no competing interests.

References

1. Floss HG, Yu TW. Rifamycin-mode of action, resistance, and biosynthesis. Chem Rev. 2005;105:621–32.
2. Kupchan SM, Komoda Y, Court WA, Thomas GJ, Smith RM, Karim A, et al. Maytansine, a novel antileukemic ansa macrolide from Maytenus ovatus. J Am Chem Soc. 1972;94:1354–6.
3. Sasaki K, Rinehart KL Jr, Slomp G, Grostic MF, Olson EC. Geldanamycin. I. structure assignment. J Am Chem Soc. 1970;92:7591–3.
4. Kang Q, Shen Y, Bai L. Biosynthesis of 3,5-AHBA-derived natural products. Nat Prod Rep. 2012;29:243–63.
5. Campbell EA, Korzheva N, Mustaev A, Murakami K, Nair S, Goldfarb A, et al. Structural mechanism for rifampicin inhibition of bacterial rna polymerase. Cell. 2001;104:901–12.
6. Artsimovitch I, Vassylyeva MN, Svetlov D, Svetlov V, Perederina A, Igarashi N, et al. Allosteric modulation of the RNA polymerase catalytic reaction is an essential component of transcription control by rifamycins. Cell. 2005;122:351–63.
7. Ramaswamy S, Musser JM. Molecular genetic basis of antimicrobial agent resistance in Mycobacterium tuberculosis: 1998 update. Tuber Lung Dis. 1998;79:3–29.
8. Siu GK, Zhang Y, Lau TC, Lau RW, Ho PL, Yew WW, et al. Mutations outside the rifampicin resistance-determining region associated with rifampicin resistance in Mycobacterium tuberculosis. J Antimicrob Chemothe. 2011;66:730–3.
9. Ye F, Zhao X, Shi Y, Hu Y, Ding Y, Lu C, et al. Deciphering the timing of naphthalenic ring formation in the Biosynthesis of 8-Deoxyrifamycins. Org Lett. 2023;25:6474–78.
10. Han TY, Zhang K, Tang GL, Zhou Q. Characterizing Post-PKS Modifications of 16-Demethyl-rifamycin revealed two dehydrogenases diverting the aromatization mode of naphthalenic ring in ansamycin biosynthesis. Chin J Chem. 2022;10:9–15.
11. Ye F, Shi Y, Zhao S, Li Z, Wang H, Lu C, et al. 8-Deoxy-Rifamycin Derivatives from *Amycolatopsis mediterranei* S699 Delta rifT Strain. Biomolecules. 2020;10:1265.
12. Shi YR, Ye F, Song YL, Zhang XC, Lu CH, Shen YM. Rifamycin W Analogues from *Amycolatopsis mediterranei* S699 Delta rif-orf5 Strain. Biomolecules. 2021;11:920.
13. Xu J, Wan E, Kim CJ, Floss HG, Mahmud T. Identification of tailoring genes involved in the modification of the polyketide backbone of rifamycin B by *Amycolatopsis mediterranei* S699. Microbioloogy. 2005;151:2515–28.
14. Qi F, Lei C, Li F, Zhang X, Wang J, Zhang W, et al. Deciphering the late steps of rifamycin biosynthesis. Nat Commun. 2018;9:2342.
15. Stratmann A, Schupp T, Toupet C, Schilling W, Oberer L, Traber R. New insights into rifamycin B biosynthesis: isolation of proansamycin B and 34a-deoxy-rifamycin W as early macrocyclic intermediates indicating two separated biosynthetic pathways. J Antibiot. 2002;55:396–406.
16. Hutchinson CR, Floss HG. Biosynthesis of the ansamycin antibiotic rifamycin: deductions from the molecular analysis of the rif biosynthetic gene cluster of *Amycolatopsis mediterranei* S699. Chem Biol. 1998;5:69–79.
17. Ghisalba O, Traxler P, Fuhrer H, Richter WJ. Early intermediates in the biosynthesis of ansamycins. II. Isolation and identification of proansamycin B-M1 and protorifamycin I-M1. J Antibiot. 1979;32:1267–72.
18. Zhang J, Li S, Wu X, Guo Z, Lu C, Shen Y. Nam7 hydroxylase is responsible for the formation of the naphthalenic ring in the biosynthesis of neoansamycins. Org Lett. 2017;19:2442–45.

19. Zhou Q, Luo G-C, Zhang H, Tang G-L. 34a-Hydroxylation in Rifamycin biosynthesis catalyzed by cytochrome P450 encoded by rif-orf13. Chin J Org Chem. 2019;39:58–63.
20. Shi Y, Zhang J, Tian X, Wu X, Li T, Lu C, et al. Isolation of 11,12-*seco*-Rifamycin W Derivatives Reveals a Cleavage Pattern of the Rifamycin Ansa Chain. Org Lett. 2019;21:900–03.
21. Li S, Lu C, Ou J, Deng J, Shen Y. Overexpression of hgc1 increases the production and diversity of hygrocins in *Streptomyces sp*. LZ35. RSC Adv. 2015;5:83843–46.
22. Zhao GS, Li SR, Guo ZX, Sun MW, Lu CH. Overexpression of div8 increases the production and diversity of divergolides in *Streptomyces sp* W112. Rsc Adv. 2015;5:98209–14.
23. Wang J, Li W, Wang H, Lu C. Pentaketide Ansamycin Microansamycins A-I from *Micromonospora sp*. Org Lett. 2018;20:1058–61.
24. Xiao YS, Zhang B, Zhang M, Guo ZK, Deng XZ, Shi J, et al. Rifamorpholines A–E, potential antibiotics from locust-associated actinobacteria *Amycolatopsis sp*. Hca4. Org Biomol Chem. 2017;15:3909–16.